Acta Materialia 188 (2020) 733–739

Contents lists available at ScienceDirect

Acta Materialia

journal homepage: www.elsevier.com/locate/actamat

Full length article

Additive manufacturing of heavy rare earth free high-coercivity permanent magnets

A.S. Volegov[a,b], S.V. Andreev[a], N.V. Selezneva[a], I.A. Ryzhikhin[a], N.V. Kudrevatykh[a], L. Mädler[c,d], I.V. Okulov[a,c,d,*,**]

[a] Institute of Natural Sciences and Mathematics, Ural Federal University, 620002 Yekaterinburg, Russia
[b] Institute of Metal Physics, Ural Division of the Russian Academy of Sciences, 620219 Yekaterinburg, Russia
[c] Faculty of Production Engineering, University of Bremen, Badgasteiner Str. 3, Bremen 28359, Germany
[d] Leibniz Institute for Materials Engineering - IWT, Badgasteiner Str. 3, Bremen 28359, Germany

ARTICLE INFO

Article History:
Received 9 December 2019
Revised 24 February 2020
Accepted 24 February 2020
Available online 27 February 2020

Keywords:
Additive manufacturing
NdFeB magnets
Coercivity
Grain boundary infiltration
Grain boundary engineering
Intergrain Exchange Interaction

ABSTRACT

Laser based powder bed fusion is a promising manufacturing method that can be used for the fabrication of hard magnets such as NdFeB with nearly any given geometrical shape. However, the weak performance, e.g., low coercivity, of the 3D-printed magnets currently hinder their application. In this work, we demonstrated a proof-of-concept of powder bed additive manufacturing of heavy rare earth free NdFeB magnets with technologically attractive coercivity values. The 3D-printed NdFeB magnets exhibit the highest (up-to-date for the additively manufactured magnets without heavy rare earth metals) coercivity values reaching $\mu_0 H_c$ = 1.6 T. The magnets were synthesized using a mixture of the NdFeB-based and the low-melting eutectic alloy powders. The essential function of the eutectic alloy, along with binding of the NdFeB-based magnetic particles, is the significant improvement of their coercivity by the *in-situ* grain boundary (GB) infiltration. The fundamental understanding of the magnetization reversal processes in these 3D-printed magnets leads to the conclusion that the excellent performance of the additively manufactured hard magnets can be achieved through the delicate control of the intergrain exchange interaction between the grains of the $Nd_2Fe_{14}B$ phase.

1. Introduction

The development of energetics and robotics, miniaturization of existing high-tech devices as well as electric and hybrid vehicles require an annual increase in the production volume of permanent magnets and at the same time improvement of their magnetic properties. Due to eddy currents, the temperature of permanent magnets used in generators and electric motors, exceeds room temperature and often reaches up to 400 K. In the case of soft magnetic materials, the eddy currents can be decreased by designing their topological structure [1]. However, this approach is unsuitable for rare earth magnets because of their high brittleness. The high temperature coefficient of coercivity limits the torque and power density of the devices at operating temperatures. Increasing the coercivity is the most important task when modifying permanent magnets. The use of grain boundary (GB) infiltration with a second material such as Cu-based alloys [2] can prevent the co-operative magnetization reversal of permanent magnet grains. This method is free of the addition of expensive heavy rare earth metals such as Tb and Dy to the permanent magnet alloy and leads to an approximately double increase in coercivity [2]. The NdFeB magnets are mainly produced by sintering that enables simple shapes such as cylinders, rings, balls, etc. Widely used magnetic systems also consist of soft-magnet elements, which act as magnetic flux "conductors" and concentrators. Recently, application of additive manufacturing technologies allowed to create magnets of more complex shapes [3] and, thus, to abandon application of soft magnetic "ballast" in magnetic cores of magnetic system.

There are several additive manufacturing techniques used to produce permanent magnets: fused deposition modelling [4,5], binder jetting [6,7] as well as laser powder bed fusion including selective laser melting [3] and selective laser sintering [8]. In the case of fused deposition modelling, a mixture of the rapidly quenched NdFeB-based alloys (MQP brand) and polymer binder were used. The significant amount of the non-magnetic polymer reaching up to 50% volume reduces the residual magnetization of this magnet by half and its $(BH)_{max}$ four times. In the recently reported highly dense isotropic

* Corresponding author at: Leibniz Institute for Materials Engineering - IWT and Faculty of Production Engineering, University of Bremen, Badgasteiner Str. 3, Bremen 28359, Germany.
** Corresponding author at: Institute of Natural Sciences and Mathematics, Ural Federal University, 620002 Yekaterinburg, Russia.
E-mail address: okulovilya@yandex.ru (I.V. Okulov).

https://doi.org/10.1016/j.actamat.2020.02.058

NdFeB nylon bonded magnets, the lowest amount of binder material is about 30% [9]. Moreover, usage of polymers limits the maximum operating temperature of such magnets. This problem can be eliminated by binder jetting where the binder material is metal [7]. However, the residual porosity leads to somewhat lower magnetic properties as compared with fully dense magnets. One of the promising additive manufacturing technology for production of fully dense and all-metal magnets is laser powder bed fusing. Unfortunately, full remelting of a special commercial NdFeB-based powder (MQP-S supplied by Magnequench Corporation) ruins its unique nanocrystalline microstructure and, thus, leads to a decrease in coercivity together with $(BH)_{max}$ values [3]. The MQP-S powder was originally designed for the manufacture of bonded magnets particularly by injection molding and extrusion. Recently, it has been demonstrated that selective laser sintering (instead of melting) is a possible manufacturing process for fabrication of NdFeB-based magnets using the MQP-S powder. To improve the low coercivity in these additively sintered magnets, the GB infiltration of the low melting alloys such as PrCu was applied as a second manufacturing step [8].

On one side, application of the grain boundary (GB) infiltration technique to a nanocrystalline NdFeB-based material leads to higher coercivity values. On the other side, introduction of paramagnetic material into the NdFeB-based material results in lower magnetization values. Since the amount of infiltrated paramagnetic material is proportional to the area of grain boundaries, it can be reduced using NdFeB-based materials with a coarser grain size. This research work is devoted to establish a single step additive manufacturing process enabling the fabrication of *in-situ* (upon 3D-printing) infiltrated NdFeB-based magnets with high coercivity values. The GB infiltration takes place during 3D-printing. Moreover, the effect of grain size of the NdFeB initial material on the final magnetic performance is discussed. For that reason, the NdFeB-based material with two different average grain sizes are selected, namely, nano- and microcrystalline.

2. Materials and methods

The schematic of the powder bed additive manufacturing process applied in this work is shown in Fig. 1. In the current experiment a mixture of two powder materials, namely, the MQP-B grade rapidly quenched alloy [10] and the $(Pr_{0.5}Nd_{0.5})_3(Cu_{0.25}Co_{0.75})$ low melting eutectic alloy [2], is used. The MQP-B powder is NdFeB-based hard magnetic material and it is studied in two conditions, namely, as-delivered (nanocrystalline) and after additional annealing at 1273 K (microcrystalline). The grain sizes of the as-delivered (nanocrystalline) and annealed (microcrystalline) magnetic material are about 25 nm and 450 nm [10], respectively. The $(Pr_{0.5}Nd_{0.5})_3(Cu_{0.25}Co_{0.75})$ material is an GB infiltration alloy to improve coercivity of the hard magnetic material. The mixture consists of 80 wt.% of the MQP-B powder and 20 wt.% of the eutectic alloy and is premixed in alcohol to avoid oxidation. The mixture was distributed manually on a Cu-based plate with 1 mm deep cavity. The as-distributed material is placed into the chamber of the additive manufacturing device (Aconity mini, Aconity3D, Germany) filled with argon gas. The speed of laser beam scanning and the number of passes were varied. The magnetic properties were measured using MPMS XL 7 EC (Quantum Design, USA) in magnetic fields of up to $\mu_0 H$ = 7 T. The demagnetization factor was about $N \approx 0.05$. The microstructural characterization was conducted using an electronic microscope using backscattered detector (Gemini Supra 40, Carl Zeiss, Germany).

3. Results and discussion

Here, we aim to prove the concept of one-step additive manufacturing process of permanent magnets with high coercivity. For this purpose, the low-melting eutectic alloy powder based on 3d-4f metals was mixed with the NdFeB-based alloy. The eutectic alloy performs two functions, namely, (i) a binder function to create a permanent magnet body from the powder and (ii) an effective separation function of nanoscale grains of the main hard magnetic phase that suppresses the exchange interaction between the grains contributing to the increase in coercivity of such a magnet. For this purpose, two powder mixtures consisting of the MQP-B alloy powder and 20 wt.% of the $(Pr_{0.5}Nd_{0.5})_3(Cu_{0.25}Co_{0.75})$ eutectic alloy were prepared. The first mixture consists of the microcrystalline MQP-B alloy (annealed at 1273 K) state. Annealing of the MQP-B alloy pursues the following goals as a result of grain coarsening: (i) change the processes of magnetization; (ii) decrease grain boundary density to reduce the required amount of the infiltrated eutectic alloy; (iii) determine the influence of grain contacts on the coercivity formation. The second mixture consists of the nanocrystalline MQP-B alloy (as-delivered state). The powder mixtures were processed with the selective laser melting method (SLM) as described in Materials and Methods. As a result, single-layer probes were synthesized to minimize the demagnetization factor in subsequent measurements of magnetic properties. The laser parameters were adjusted to achieve melting of the eutectic alloy and simultaneously avoid the melting of the hard magnetic alloy. For this reason, the laser beam diameter was increased from about 50 μm to 100 μm to establish a more homogeneous heat distribution and to suppress a local overheating of the powder mixtures.

The phase composition of the 3D-printed nano- and microcrystalline magnets was probed by the X-Ray analysis. The exemplified X-ray pattern of the 3D-printed nanocrystalline magnet are shown in Fig. 2. According to the Rietveld refinement, the upper surface layer (the one facing laser beam) of the 3D-printed nanocrystalline magnet consists of the initial $Nd_2Fe_{14}B$ magnetic phase as well as several new phases including α-Fe, $(Nd, Pr)_2O_3$ and $(Nd, Pr)(OH)_3$ phases (Fig. 2a). The X-ray analysis of the powdered sample indicates also formation of the $(Nd,Pr)Fe_4B_4$ phase (Fig. 2b). The lattice parameters and space group of the phases are listed in Table 1. The formation of $(Nd, Pr)_2O_3$ phase is due to high reactivity of Nd and Pr with oxygen. To prevent the oxidation of Nd and Pr, the initial powder mixtures were stored in alcohol. The powder mixtures wetted with the alcohol were distributed on the platform for the SLM processing. Since the presence of the initial eutectic material was undetected in the 3D-printed magnets, it is reasonable to conclude that the NdPr-based eutectic

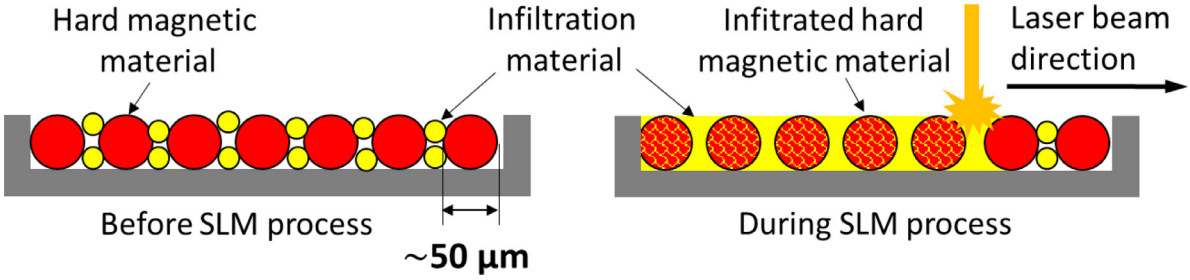

Fig. 1. Schematic illustration of the additive manufacturing of high-coercivity permanent magnets via one-step process.

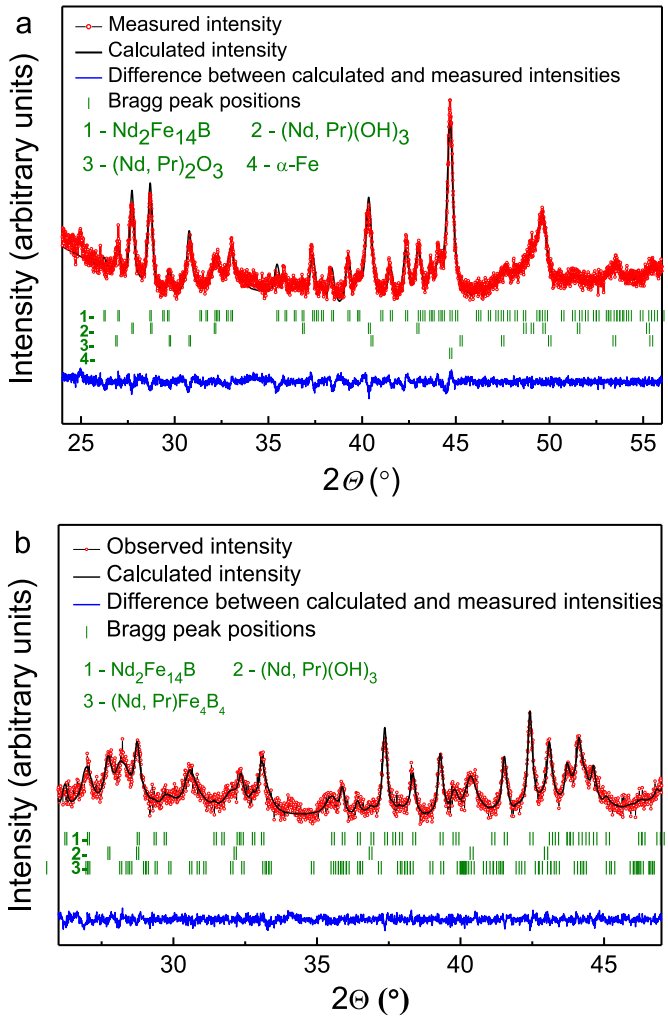

Fig. 2. X-Ray diffraction patterns (measured and calculated) of the 3D-printed nanocrystalline magnet: (a) upper surface of the as-printed sample and (b) powdered sample obtained from the 3D-printed magnet.

material has chemically reacted during the SLM process to form (Nd, Pr)$_2$O$_3$ and (Nd, Pr)(OH)$_3$. The formation of α-Fe was expected since this is a decomposition product of $Nd_2Fe_{14}B$ subjected to elevated temperatures above the certain threshold in the presence of oxygen and hydroxide [11].

The microstructural analysis combined with the EDX analysis prove the presence of microscale Fe-rich crystals (dark areas) located in the upper layer of the 3D-printed nanocrystalline magnet (Fig. 3a). It seems that the diffusion of the NdPr-based alloy into the $Nd_2Fe_{14}B$-based particles leads to the dealloying effect [12–20], namely, diffusion of Nd from the $Nd_2Fe_{14}B$ phase into the NdPr-based phase. Upon dealloying, the $Nd_2Fe_{14}B$ phase is locally depleted in Nd (but enriched in Fe) and, eventually, transforms into α-Fe. The dealloying process is time and temperature limited process [18,21] and, therefore, the middle and bottom layers of the 3D-printed magnets are α-Fe-free.

Table 1
Phases observed in the 3D-printed nanocrystalline magnets.

Phase	Space group	Lattice parameters (Å)
$Nd_2Fe_{14}B$	$P4_2/mnm$	a = 8.798(3) c = 12.156(4)
α-Fe	Im-3m	a=2.8664
(Nd, Pr)O_3	P-3m1	a=3.8297 c=6.01
(Nd, Pr)$(OH)_3$	$P6_3/m$	a=6.432 c=3.742
$(Nd,Pr)Fe_4B_4$	Pccn	a=7.117(1) c= 35.070(5)

This was proven with X-ray (Fig. 2b) and SEM analyses (Fig. 3). The microstructure of the 3D-printed magnets possesses a gradient structure, namely, an increase in grain size of the hard magnetic phase in the direction from the bottom to the top direction. Ca. 200 μm below the upper layer, the size of the $Nd_2Fe_{14}B$ phase reduces from about 3 μm to about 1 μm and a typical morphology of the infiltrated $Nd_2Fe_{14}B$ materials can be observed (Fig. 3b). The most grains have a direct contact to each other. The $Nd_2Fe_{14}B$ grains (darker areas) are distinctly separated by the other phase(s) appearing as brighter areas. The microstructural gradient is due to a limited heat transfer from the top towards the bottom layer of the sample. In other words, the upper layer experienced longer heat treatment at higher temperatures as compared with the bottom layer.

The 3D-printed nanocrystalline magnet synthesized from the MQP-B (nanocrystalline) in the as-delivered condition exhibits much finer gradient microstructure compared to the 3D-printed microcrystalline magnet (Fig. 4). The size of the $Nd_2Fe_{14}B$ grains in the upper layer is ca. 200 nm (Fig. 4b) what is about 5 times smaller than that of the microcrystalline magnet. In the layer ca. 150 μm below the upper surface, the grain size decreases below 100 nm (Fig. 4c and d). The distinct dark-grey areas of the $Nd_2Fe_{14}B$ grains separed by the phases appearing as brighter areas is observed in every micrograph presented in Fig. 4. This bright areas are probably due to the $NdFe_4B_4$, (Nd, Pr)$_2$O$_3$ and (Nd, Pr)$(OH)_3$ phases detected in the XRD patterns. The $Nd_2Fe_{14}B$ grains are separated by (Nd, Pr)$_2$O$_3$ and (Nd, Pr)$(OH)_3$. In the near-bottom layer (ca. 500 μm from the surface), separation of the $Nd_2Fe_{14}B$ grains by the paramagnetic eutectic alloy was undetected by SEM analysis. To minimize the effect of gradient microstructure on magnetic properties, the upper and lower layers of the 3D-printed samples were removed by mechanical polishing.

Major hysteresis loops of initial alloys and 3D-printed magnets are presented in Fig. 5. The coercivity $\mu_0 H_c$ of the 3D-printed nano- and microcrystalline magnets demonstrate significant improvement (increased in 1.7 and 18.4 times, respectively) compared with that of the initial (nanocrystalline) and the heat treated (microcrystalline) MQP-B powders (Fig. 5). The coercivity values of 3D-printed nano- and microcrystalline magnets are 1.6 T and 0.92 T, respectively. The improvement in coercivity of the 3D-printed microcrystalline magnets is associated with the decrease of the number of grain boundary defects as compared to the microcrystalline MQP-B powder. According to the SEM analysis (Fig. 3b), there are many non-infiltrated, i.e., free of the paramagnetic layer, regions in the 3D-printed microcrystalline magnet. It is assumed that the GB infiltration occurs through those junctions where the local atomic surrounding exhibits a highly non-equilibrium configuration. These non-equilibrium configurations are due to the growth of grains possessing random crystallographic orientation. The grain boundary near Nd atoms experience crystal-electric fields of low symmetry leading to the local decrease in magnetocrystalline anisotropy and, thus, a high possibility of the domain nucleation with the reversal magnetization. Once the domain wall is formed, it can freely move within the grains through shared boundaries [22]. The paramagnetic alloy diffused through the grain boundaries induced their “repairing”, i.e., reduction of the number of defects. In its turn, this causes the local increase of the constant of anisotropy and the multiple increase in coercivity of the current additively manufactured magnets.

The coercivity of the heat treated MQP-B powder is about $\mu_0 H_c$ = 0.05 T while the coercivity of the initial MQP-B powder is 0.94 T. The highly coercive state of the nanocrystalline MQP-B material with a characteristic grain size of 25 nm [10] is due to the irreversible rotation of the magnetization in the nanograins. The formation of a domain wall, in this case, is energetically disadvantageous because the grain size is too small. The decrease in coercivity is associated with the following aspects: first, change in the process of magnetization reversal from the irreversible rotation of magnetization (initial MQP-B) to the nucleation (heat treated MQP-B) and, second, the high number of defects at the grain boundary regions leading to a local

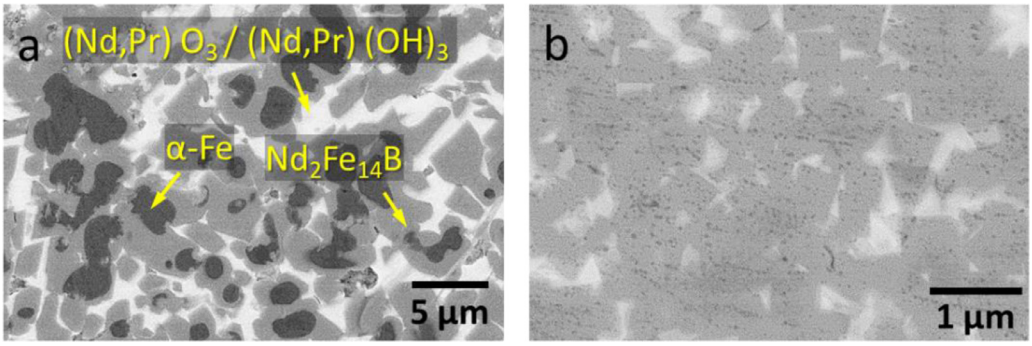

Fig. 3. SEM micrographs of the 3D-printed microcrystalline magnet (microcrystalline magnet is synthesized from a mixture of the microcrystalline MQP-B powder and low melting eutectic alloy) through its thickness to demonstrate gradient microstructure. (a) microstructure of the upper layer; (b) microstructure in the layer ca 200 μm below the upper surface.

decrease in the field of anisotropy (heat treated MQP-B). Finally, the latter leads to decrease in the magnetic field required for the formation of nucleus of magnetization reversal.

The intergrain exchange interaction between the grains with shared grain boundary as well as a high number of defects at the grain boundary lead to the decrease in the effective constant of anisotropy similar to that in soft magnetic materials [23] and, therefore, decrease in coercivity far below the theoretical limit (H_c = 0.479 H_a where $H_a \approx 8$ T at room temperature – field of anisotropy of the $Nd_2Fe_{14}B$ phase) predicted within the Stoner–Wohlfarth model [24]. The increase in coercivity after 3D-printing in the case of the nanocrystalline magnet is due to a decrease in the average value of the intergrain exchange interaction constant which will be shown below.

There is a significant difference in shape of the hysteresis loops between the nanocrystalline 3D-printed magnet and the original MQP-B material. Particularly, the hysteresis loop of the initial powder shows high rectangularity. The hysteresis loops of the 3D-printed nanocrystalline magnet possess a less rectangular loop shape close to that of the isotropic Stoner–Wohlfarth ensemble [25], with a slow decrease in magnetization in the magnetic fields of less than the coercivity and a sharp change in the fields slightly exceeding the latter. Such a difference is attributed to the suppression of intergrain exchange interaction of composite $Nd_2Fe_{14}B$-based materials due to the paramagnetic layer between grains [26]. The hysteresis loop of the 3D-printed microcrystalline magnet is also not rectangular and possesses some inflection. Such form of the hysteresis loop is associated with the wide distribution of nucleation fields of the different areas/places of the sample. Based on the field value, the inflections are probably due to the remaining non-infiltrated zones of the initial $Nd_2Fe_{14}B$ material or zones with large area of a direct contact between neighbor grains (Figs. 3b and 4d).

Comparing magnetic behaviour of the 3D-printed magnets, it is important to point out that both samples types, nano- and microcrystalline magnets, contain the same amount of the paramagnetic GB infiltration alloy but their coercivity values differ 1.7 times. This is related with their microstructure and, specifically, the grain size. The GB infiltration alloy and the hard magnetic phase form percolated areas in the microcrystalline magnet. In this case, domain walls can move easily from grain to grain between coupled grains with the shared boundary or junction points (Fig. 3b). A single location with the reduced local anisotropy (e.g., near the defect) is enough to start magnetization reversal in a few hundreds or thousands of cubic microns of the sample. In contrary to the 3D-printed microcrystalline magnet, according to the SEM analysis, the 3D-printed nanocrystalline magnet

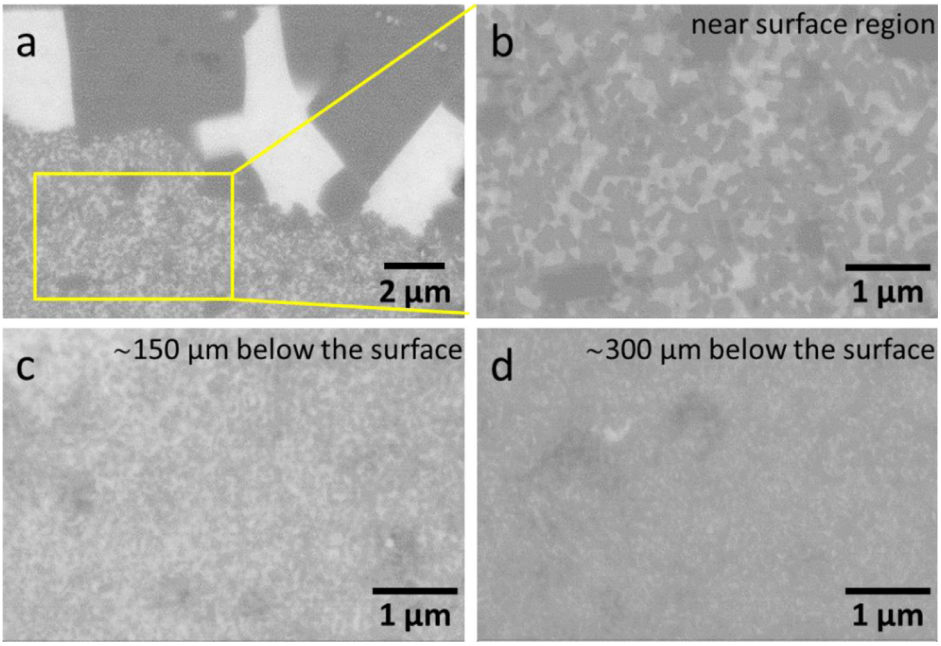

Fig. 4. SEM micrographs of the 3D-printed nanocrystalline magnet (nanocrystalline magnet is synthesized from a mixture of the nanocrystalline MQP-B powder and the low melting paramagnetic eutectic alloy) to demonstrate its gradient microstructure. (a) and (b) microstructure of the upper layer; (c) microstructure in the layer ca. 150 μm below the upper surface; and (d) microstructure in the layer ca. 300 μm below the upper surface.

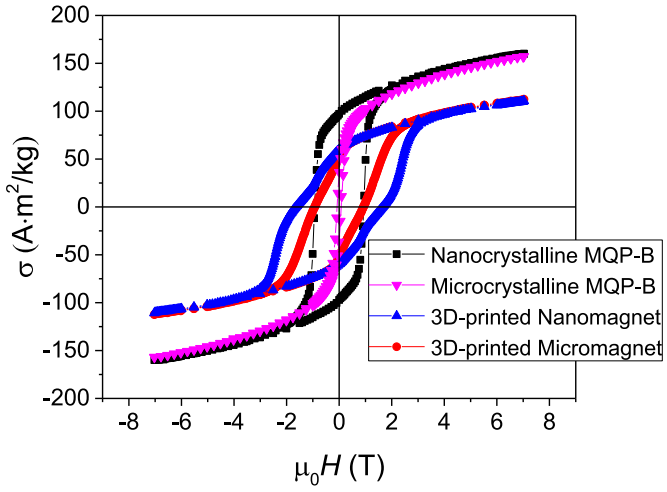

Fig. 5. Major hysteresis loops of the initial nanocrystalline and the annealed microcrystalline MQP-B materials as well as 3D-printed nano- and microcrystalline magnets at T = 300 K (Note: Nanomagnet – nanocrystalline magnet and Micromagnet – microcrystalline magnet).

possesses relatively small areas of coupled grains. Due to the fine grain size, the existence of domain wall in the grains of the nanocrystalline magnet is unlikely. In this case, magnetization reversal occurs through the irreversible rotation of the magnetization vector and percolation is the insufficient condition for the magnetization reversal of large areas in the nanocrystalline magnet. Decreasing of the grain contact area leads to the diminution of cooperative magnetization reversal and the increasing of coercivity values.

The magnets are typically operated in a wide temperature range. Therefore, temperature dependence of coercivity of the 3D-printed $Nd_2Fe_{14}B$-based magnets was measured and presented in Fig. 6. The temperature coefficients of coercivity β (sensitivity of magnet coercivity to temperature changes) are shown in the second column of Table 2. The absolute value of β increases with increasing grain size in the current 3D-printed magnets, what was previously observed for the hot deformed NdFeB anisotropic magnets [27]. This indicates that the 3D-printed microcrystalline magnets are more sensitive to temperature as compared with the nanocrystalline ones. More importantly, coercivity of the current 3D-printed nanocrystalline magnets is less dependent on temperature as compared with the sintered magnets [27–29].

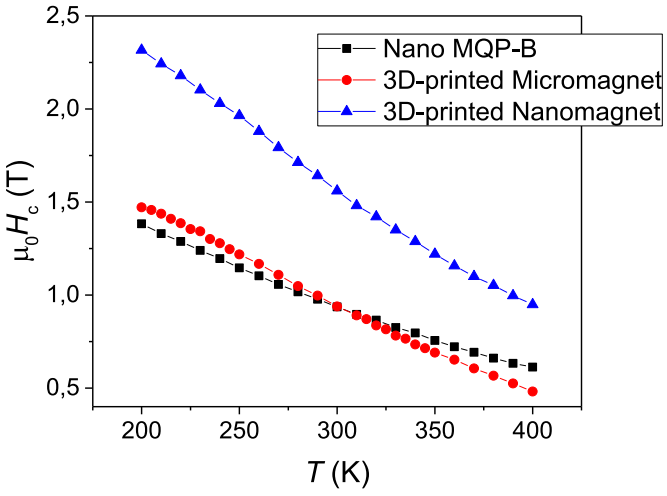

Fig. 6. Coercivity vs. temperature dependence of the initial nanocrystalline MQP-B material and 3D-printed nano- and microcrystalline magnets at temperature range 200–400 K.

Table 2
Temperature coefficients of coercivity β, remanence magnetization, spontaneous magnetization and their ratio of the initial nanocrystalline MQP-B material and 3D-printed nano- and microcrystalline magnets.

Sample	β (%/K)	σ_r (A·m²/kg)	σ_s (A·m²/kg)	σ_r/σ_s
3D-printed microcrystalline magnet	– 0.55	59.4	118.6	0.50
3D-printed nanocrystalline magnet	– 0.44	60.5	120.6	0.50
Initial MQP-B	– 0.42	96.1	171.4	0.56

The ratio of coercivity values of the nanocrystalline magnet and the initial MQP-B powder H_c^B/H_c^{MQP-B} is about 1.7 for all temperatures. This means that the 3D-printed permanent magnets produced by the proposed process can withstand a higher magnetic field as compared with the original material without magnetization reversal. The recently reported ratio of coercivity of heavy rare earth free additively manufactured $Nd_2Fe_{14}B$-based magnets and initial powder material H_c^{final}/H_c^{MQP-S} obtained by two-stage process is about 1.15 [8]. The addition of heavy rare earth elements can improve the coercivity ratio up to the value of about 1.7 [8]. However, the application-relevant absolute coercivity value of our nanocrystalline magnet (1.6 T) is higher than that of this 3D-printed magnet (1.5 T) from reference [8]. The absolute coercivity value of our 3D-printed magnets is about 35% higher as compared to the literature results for the heavy rare earth free 3D-printed magnets.

To estimate the influence of the formed intergrain layer on the weakening of the grain exchange interaction, the ratio of residual magnetization to spontaneous magnetization was determined. In the absence of interaction between the particles, this ratio is 0.5 for the isotropic Stoner–Wohlfarth ensemble. The comparison of the considered 3D-printed magnets with this model in positive applied magnetic field is correct due to isotropic distribution of easy magnetization axes of the main hard magnetic $Nd_2Fe_{14}B$ phase and absence of irreversible magnetization reversal. Table 2 presents the values of residual and spontaneous magnetization obtained from the law of approaching to magnetic saturation. The initial alloy MQP-B shows the largest deviation from the Stoner–Wohlfarth limit caused by strong intergrain exchange interaction of ferromagnetic type. The relative residual magnetization of the 3D-printed nanocrystalline magnet is fully consistent with the Stoner–Wohlfarth model. The hysteresis loop of the 3D-printed microcrystalline magnet exhibits an inflection near the zero magnetic field strength and the value of residual magnetization was determined in zero internal magnetic field.

For an independent quantitative evaluation of the intergrain exchange interaction in the 3D-printed magnets, the method based on the comparison of temperature dependencies of their residual magnetization was used [30]. Before starting the measurement, the 3D-printed magnets were magnetized in the magnetic field $\mu_0 H$ = 7 T at room temperature. The temperature dependence of the residual magnetization upon cooling was measured after switching off the magnetic field. Fig. 7 shows the dependence of residual magnetization at T = 300 K. The 3D-printed magnets are affected by their own demagnetization field of $\mu_0 H_d$ ~ 0.02 - 0.04 T. Spontaneous magnetization and, accordingly, residual magnetization increase upon temperature decrease from 300 to 135 K. At temperature of $T_{sr} \approx$ 135 K, there is the spontaneous spin-reorientation transition in the 3D-printed magnets. The type of this transition is the easy magnetization axis - the cone of easy magnetization axes. Below $T_{sr} \approx$ 135 K, the dependences change radically. The 3D-printed microcrystalline magnet shows a decrease in magnetization. This is due to a deviation of magnetic moments of individual crystallites from the direction of the residual magnetization to minimize the magnetostatic energy in their own demagnetization field. The temperature dependence of the reduced residual magnetization of the initial MQP-B alloy near T_{sr} is deflected in the opposite direction. The reason

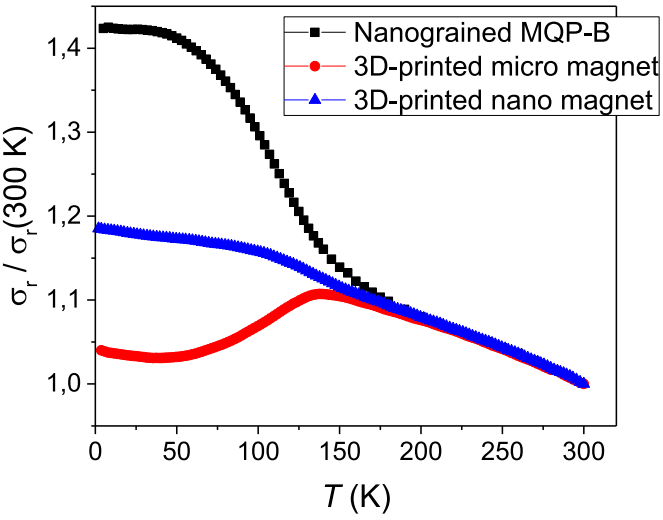

Fig. 7. Reduced remanence vs. temperature dependence of the initial nanocrystalline MQP-B material and 3D-printed nano- and microcrystalline magnets (Note: Nanomagnet – nanocrystalline magnet and Micromagnet – microcrystalline magnet).

for such behaviour is a strong intergrain exchange interaction of the ferromagnetic type which is prevailing over the magnetostatic one. The parallel orientation of magnetic moments of the neighboring grains is energetically advantageous for this interaction. Based on the current curves (Fig. 7), it can be concluded that the exchange interaction in the MQP-B alloy prevails over the magnetostatic one. At the same time, the magnetostatic interaction prevails over the exchange one in the 3D-printed microcrystalline magnet. This is associated with a small specific contact area of neighboring grains and the presence of intergrain paramagnetic layer suppressing the exchange interaction. The position of magnetic moments at the phase transition remains the same allowing to estimate a constant of intergrain exchange interaction quantitatively within the limits of the approximation given below.

The energy of intergrain exchange interaction in the 3D-printed nanocrystalline magnet can be written in the following form:

$$E = -K_{ex} S \overline{\cos}\phi,$$

where K_{ex} –constant of intergrain exchange interaction, S – contact area between grains, $\overline{\cos}\phi$ – mean angle cosine value between magnetic moments of neighboring grains.

In the state of residual magnetization and in the case of uniaxial type of magnetocrystalline anisotropy $\overline{\cos}\phi \approx 0.25$.

Interaction energy of magnetic moments with their own demagnetization field:

$$E_d = -\mu_0 N V M_r M_s \cos(\theta),$$

where N–demagnetization factor of the 3D-printed nanocrystalline magnet $(N = 0.05)$, V–volume of a crystal, M_s – spontaneous magnetization of $Nd_2Fe_{14}B$ intermetallic $(M_s = 1.27\text{MA/m})$, M_r– remanent magnetization of the 3D-printed nanocrystalline magnet $(M_r \approx 0.32\text{MA/m})$, θ – angle between directions of magnetic moment of a grain and demagnetizing field $(\overline{\cos}\,\theta \approx 0,5)$.

Then, assuming the cubic form of particles and equality of these energies:

$$K_{ex} = \frac{\mu_0 N d M^2 \cos(\theta)}{\overline{\cos}\phi} \approx 1.5 \text{ mJ/m}^2,$$

where d–mean value of the grain size $(\overline{d} \approx 30\text{nm})$ derived from the measured here XRD diffractograms.

From the fundamental point of view, the determination of the numerical value of K_{ex} in the magnetic materials of the NdFeB system at different thicknesses of the paramagnetic layer is essential for understanding of the magnetization reversal processes in both nano- and microcrystalline (sintered) magnets. In the latter case, the increase in thickness of the paramagnetic layer leads to the increase in coercivity values what is associated with the decrease in the K_{ex} values between grains and their independent magnetization reversal. Additionally, the K_{ex} value together with the data on microstructure and magnetic hysteresis properties provide the information about the area of preserved contacts between grains. As an important practical implication, understanding the dependence of intergrain exchange interaction with respect to the chemical composition of the intergrain paramagnetic layer enables purposeful composition optimization of this layer in order to minimize its volume while maintaining high values of residual magnetization.

Value K_{ex} is about 5–7 times lower than the same one estimated in [20,24,25,31,32]. The positive value of K_{ex} is determined by the intergrain exchange interaction through the remaining contact areas between the grains. Varying K_{ex} allows local tuning of magnetic properties in permanent magnets or magnetic systems. In the area of poles, K_{ex} can be like in the initial material while in other parts it can be reduced to increase coercivity. Additionally, the stray field free systems can be designed by fine control of magnetic flux through the different parts of a magnetic system. The stray field free magnetic systems will possess small weight and volume.

4. Summary

In this work we demonstrated feasibility of the single step additive manufacturing of the heavy rare earth free high-coercivity NdFeB magnets with the coercivity up to 1.6 T. This was possible due to integration of the *in-situ* grain boundary (GB) infiltration of the low melting paramagnetic alloy (between the grains of the $Nd_2Fe_{14}B$ phase) into the additive manufacturing process. To understand the influence of microstructure and magnetization reversal processes on the hysteresis magnetic properties of the 3D-printed magnets, nano- and microcrystalline magnets were synthesized. It was found that the microcrystalline magnets demonstrate lower coercivity in comparison with that of the nanocrystalline ones. This is due to the existence of the large areas of magnetically coupled grains with shared boundaries in the 3D-printed microcrystalline magnets. Due to the coupled grains, the domain wall can easily move through the shared boundaries leading to reduction in coercivity. It was experimentally demonstrated that decreasing the average intergrain exchange interaction by reducing the area of shared grain boundaries, in the case of the 3D-printed nanocrystalline magnets, results in significant (1.7 times as compared with that of the 3D-printed microcrystalline magnets) increase in coercivity. The decoupling of grains is achieved by addition of the paramagnetic layer between the $Nd_2Fe_{14}B$ grains leading to the reduction of the exchange interaction constant value. Within the limits of the model of irreversible rotation of magnetization, the increase in coercivity is due to the increase of the effective constant of anisotropy associated with the decrease in the average number of neighboring grains having shared boundaries. It is shown that the temperature coefficient of coercivity of the 3D-printed magnets is lower than that of the microcrystalline ones due to the different mechanisms of magnetization reversal. Both technological know-how and fundamental understanding of the magnetization reversal processes of the 3D-printed magnets demonstrated in this work pave the way for the additive manufacturing of high-coercivity and low-weight magnetic systems without heavy rare earth elements.

Declaration of Competing Interest

The authors declare that they have no known competing financial interests or personal relationships that could have appeared to influence the work reported in this paper.

Acknowledgment

The financial support was provided by the German Science Foundation under the Leibniz Program (Grant MA 3333/13-1), by Act 211 Government of the Russian Federation (contract № 02.A03.21.0006), and Ministry of Science and Higher Education of the Russian Federation, Grant Number FEUZ-2020-0051.

References

[1] D. Goll, D. Schuller, G. Martinek, T. Kunert, J. Schurr, C. Sinz, T. Schubert, T. Bernthaler, H. Riegel, G. Schneider, Additive manufacturing of soft magnetic materials and components, Addit. Manuf. 27 (2019) 428–439, doi: 10.1016/j.addma.2019.02.021.

[2] R. Madugundo, D. Salazar-Jaramillo, J. Manuel Barandiaran, G.C. Hadjipanayis, High coercivity in rare-earth lean nanocomposite magnets by grain boundary infiltration, J. Magn. Magn. Mater. 400 (2016) 300–303, doi: 10.1016/j.jmmm.2015.07.019.

[3] J. Jaćimović, F. Binda, L.G. Herrmann, F. Greuter, J. Genta, M. Calvo, T. Tomše, R.A. Simon, Net shape 3D printed NdFeB permanent magnet, Adv. Eng. Mater. 19 (2017) 1–7, doi: 10.1002/adem.201700098.

[4] L. Li, A. Tirado, I.C. Nlebedim, O. Rios, B. Post, V. Kunc, R.R. Lowden, E. Lara-Curzio, R. Fredette, J. Ormerod, T.A. Lograsso, M.P. Paranthaman, Big area additive manufacturing of high performance bonded NdFeB magnets, Sci. Rep. 6 (2016) 1–7, doi: 10.1038/srep36212.

[5] C. Huber, C. Abert, F. Bruckner, M. Groenefeld, O. Muthsam, S. Schuschnigg, K. Sirak, R. Thanhoffer, I. Teliban, C. Vogler, R. Windl, D. Suess, 3D print of polymer bonded rare-earth magnets, and 3D magnetic field scanning with an end-user 3D printer, Appl. Phys. Lett. (2016) 109, doi: 10.1063/1.4964856.

[6] L. Li, A. Tirado, B.S. Conner, M. Chi, A.M. Elliott, O. Rios, H. Zhou, M.P. Paranthaman, A novel method combining additive manufacturing and alloy infiltration for NdFeB bonded magnet fabrication, J. Magn. Magn. Mater. 438 (2017) 163–167, doi: 10.1016/j.jmmm.2017.04.066.

[7] M.P. Paranthaman, C.S. Shafer, A.M. Elliott, D.H. Siddel, M.A. McGuire, R.M. Springfield, J. Martin, R. Fredette, J. Ormerod, B. Jetting, A novel NdFeB bonded magnet fabrication process, JOM 68 (2016) 1978–1982, doi: 10.1007/s11837-016-1883-4.

[8] C. Huber, H. Sepehri-Amin, M. Goertler, M. Groenefeld, I. Teliban, K. Hono, D. Suess, Coercivity enhancement of selective laser sintered NdFeB magnets by grain boundary infiltration, Acta Mater. 172 (2019) 66–71, doi: 10.1016/j.actamat.2019.04.037.

[9] L. Li, K. Jones, B. Sales, J.L. Pries, I.C. Nlebedim, K. Jin, H. Bei, B.K. Post, M.S. Kesler, O. Rios, V. Kunc, R. Fredette, J. Ormerod, A. Williams, T.A. Lograsso, M.P. Paranthaman, Fabrication of highly dense isotropic Nd-Fe-B nylon bonded magnets via extrusion-based additive manufacturing, Addit. Manuf. 21 (2018) 495–500, doi: 10.1016/j.addma.2018.04.001.

[10] A.S. Volegov, Межзеренное обменное взаимодействие в наноструктурированных сплавах системы РЗМ-3d-металл-бор и его роль в формировании их фундаментальных и гистерезисных магнитных свойств, Ural Federal University, 2012.

[11] Y. Li, H.E. Evans, I.R. Harris, I.P. Jones, The oxidation of NdFeB magnets, Oxid. Met. 59 (2003) 167–182, doi: 10.1023/A:1023078218047.

[12] P. Geslin, I. Mccue, J. Erlebacher, A. Karma, Topology-generating interfacial pattern formation during liquid metal dealloying, Nat. Commun. 6 (2015) 1–19, doi: 10.1038/ncomms9887.

[13] I.V. Okulov, P.-A. Geslin, I.V. Soldatov, H. Ovri, S.-H. Joo, H. Kato, Anomalously low modulus of the interpenetrating-phase composite of Fe and Mg obtained by liquid metal dealloying, Scr. Mater. 163 (2019) 133–136, doi: 10.1016/j.scriptamat.2019.01.017.

[14] I.V. Okulov, S.V. Lamaka, T. Wada, K. Yubuta, M.L. Zheludkevich, J. Weissmüller, J. Markmann, H. Kato, Nanoporous magnesium, Nano Res. 11 (2018) 6428–6435, doi: 10.1007/s12274-018-2167-9.

[15] T. Wada, K. Yubuta, A. Inoue, H. Kato, Dealloying by metallic melt, Mater. Lett. 65 (2011) 1076–1078, doi: 10.1016/j.matlet.2011.01.054.

[16] A.V. Okulov, A.S. Volegov, J. Weissmüller, J. Markmann, I.V. Okulov, Dealloying-based metal-polymer composites for biomedical applications, Scr. Mater. 146 (2018) 290–294, doi: 10.1016/j.scriptamat.2017.12.022.

[17] I.V. Okulov, A.V. Okulov, A.S. Volegov, J. Markmann, Tuning microstructure and mechanical properties of open porous TiNb and TiFe alloys by optimization of dealloying parameters, Scr. Mater. 154 (2018) 68–72, doi: 10.1016/j.scriptamat.2018.05.029.

[18] I. McCue, B. Gaskey, P.A. Geslin, A. Karma, J. Erlebacher, Kinetics and morphological evolution of liquid metal dealloying, Acta Mater. 115 (2016) 10–23, doi: 10.1016/j.actamat.2016.05.032.

[19] I.V. Okulov, J. Weissmüller, J. Markmann, Dealloying-based interpenetrating-phase nanocomposites matching the elastic behavior of human bone, Sci. Rep. 7 (2017) 20, doi: 10.1038/s41598-017-00048-4.

[20] S.-H. Joo, J.W. Bae, W.-Y. Park, Y. Shimada, T. Wada, H.S. Kim, A. Takeuchi, T.J. Konno, H. Kato, I.V. Okulov, Beating thermal coarsening in nanoporous materials via high-entropy design, Adv. Mater. (2020) 1906160, doi: 10.1002/adma.201906160.

[21] I.V. Okulov, A.V. Okulov, I.V. Soldatov, B. Luthringer, R. Willumeit-Römer, T. Wada, H. Kato, J. Weissmüller, J. Markmann, Open porous dealloying-based biomaterials as a novel biomaterial platform, Mater. Sci. Eng. C 83 (2018) 95–103, doi: 10.1016/j.msec.2018.03.008.

[22] I.V. Soldatov, R. Schäfer, Selective sensitivity in Kerr microscopy, Rev. Sci. Instrum. 88 (2017) 73701, doi: 10.1063/1.4991820.

[23] A.S. Bolyachkin, S.V. Komogortsev, Power-law behavior of coercivity in nanocrystalline magnetic alloys with grain-size distribution, Scr. Mater. 152 (2018) 55–58, doi: 10.1016/j.scriptamat.2018.04.008.

[24] F. Bolzoni, O. Moze, L. Pareti, First–order field–induced magnetization transitions in single–crystal Nd2Fe14B, J. Appl. Phys. 62 (1987) 615–620, doi: 10.1063/1.339789.

[25] E.C. Stoner, E.P. Wohlfarth, A mechanism of magnetic hysteresis in heterogeneous alloys, Philos. Trans. R. Soc. Lond. Ser. A Math. Phys. Sci. 240 (1948) 599–642, doi: 10.1098/rsta.1948.0007.

[26] A.S. Bolyachkin, S. Ruta, R.W. Chantrell, T.G. Woodcock, S.V. Andreev, N.V. Selezneva, A.S. Volegov, Characterisation of high-anisotropy nanocrystalline alloys based on magnetic susceptibilities in the remanent state, J. Magn. Magn. Mater. 486 (2019) 165270, doi: 10.1016/j.jmmm.2019.165270.

[27] J. Liu, H. Sepehri-Amin, T. Ohkubo, K. Hioki, A. Hattori, T. Schrefl, K. Hono, Grain size dependence of coercivity of hot-deformed Nd–Fe–B anisotropic magnets, Acta Mater. 82 (2015) 336–343, doi: 10.1016/j.actamat.2014.09.021.

[28] G. Bai, R.W. Gao, Y. Sun, G.B. Han, B. Wang, Study of high-coercivity sintered NdFeB magnets, J. Magn. Magn. Mater. 308 (2007) 20–23, doi: 10.1016/j.jmmm.2006.04.029.

[29] A.S. Kim, F.E. Camp, High performance NdFeB magnets (invited), J. Appl. Phys. 79 (2002) 5035, doi: 10.1063/1.361566.

[30] N.V. Kudrevatykh, A.S. Volegov, A.V. Glebov, S.V. Andreev, V. Pushin, P.E. Markin, D.S. Neznakhin, Microstructure and magnetic hysteresis in nanocrystalline Nd-Fe-Co-B alloys on the base of $Nd_2Fe_{14}B$ phase, Solid State Phenom. 168–169 (2010) 420–423, doi: 10.4028/www.scientific.net/ssp.168-169.420.

[31] A.S. Volegov, A.S. Bolyachkin, N.V. Kudrevatykh, A new method of intergrain exchange interaction energy determination in nanostructured alloys with spontaneous spin-reorientation transition, Solid State Phenom. 233–234 (2015) 615–618, doi: 10.4028/www.scientific.net/ssp.233-234.615.

[32] D. Ogawa, K. Koike, H. Kato, S. Mizukami, T. Miyazaki, M. Oogane, Y. Ando, Evaluation of interlayer exchange coupling in α-Fe(100)/Nd2Fe14B(001) films, J. Korean Phys. Soc. 63 (2013) 489–492, doi: 10.3938/jkps.63.489.